Chemical, Thermal, and Ultrasonic Stability of Hybrid Nanoparticles and Nanoparticle Multilayer Films

Steven R. Isaacs,† Hosun Choo,† Weon-Bae Ko,*,‡ and Young-Seok Shon*,†

Department of Chemistry, Western Kentucky University, Bowling Green, Kentucky 42101, and Department of Chemistry, Sahmyook University, Seoul 139-742, South Korea

Received August 23, 2005. Revised Manuscript Received October 31, 2005

Gold nanoparticles stabilized by thiolates derived from normal and ω-functionalized alkane- and arenethiols ($HS(CH_2)_nCH_3$, $HS(CH_2)_{10}COOH$, $HS(CH_2)_{11}OH$, $HSC_6H_4NH_2$, $HSCH_2CH_2C_6H_5$, and $HSCH_2C_6H_4C(CH_3)_3$) were synthesized. Differences in their chemical and ultrasonic stabilities were studied using UV−vis spectroscopy. The results showed that these stabilities of monolayer-protected nanoparticles were greatly influenced by the structure and functionality of the monolayer surrounding a nanoparticle core. The selective functionalization of the nanoparticle allowed us to prepare hybrid nanostructures (nanoparticle multilayer assemblies) with different compositions and functionalities. This paper also presents an investigation of the chemical, thermal, and ultrasonic treatments of these nanoparticle multilayer assemblies. The results suggest that the linkers used to build nanoparticle multilayer films govern the overall stability of hybrid nanostructures.

Introduction

Nanoparticles with a diameter of less than 10 nm have generated intense interest over the past several years.[1,2] The most significant problems with the applications of nanoparticles have been property changes over time and poor solubility due to oxidation and irreversible aggregation. The self-assembly of monolayers onto the surface of nanoparticles resulted in the formation of monolayer-protected clusters (MPCs), and enhanced the solubility and stability of the nanoparticles. Functionalized MPCs have been directly synthesized from organic compounds with different functional groups (e.g., ω-functionalized alkanethiols, mixtures of alkanethiols, unsymmetrical dialkyl disulfides, or sulfides).[1−4] Mixed monolayer-protected clusters (MMPCs) have also been synthesized from MPCs by ligand-place-exchange reactions.[1,2] MMPCs have applications in various fields of research, including catalysis,[5] films,[6] heavy-metal detection,[7] and chemical recognition.[8,9] As more technological applications of these MPCs and MMPCs are being realized, better knowledge of material properties, including the stability of MPCs and MMPCs, becomes critical for the long-term use of these materials in device applications. There have been a few reports related to studies of the chemical and thermal stability of ligand-stabilized nanoparticles.[10−15] For the expansion of knowledge on the stability of these materials, we synthesized MPCs protected with various alkanethiols or arenethiols and MMPCs containing different functional groups (−NH_2, −COOH, and −OH groups), as shown in Figure 1.

Because of the enhanced stability and versatility of these nanoparticles, MMPCs have been used for the preparation of hybrid thin films by a self-assembly process based on an interaction or a bond formation between MMPCs and linkers.[16−24] Combining the versatility of various linkers with

* To whom correspondence should be addressed. E-mail: young.shon@wku.edu (Y.-S.S.), kowb@syu.ac.kr (W.-B.K.).
† Western Kentucky University.
‡ Sahmyook University.

(1) Daniel, M.-C.; Astruc, D. *Chem. Rev.* **2004**, *104*, 293.
(2) Templeton, A. C.; Wuelfing, W. P.; Murray, R. W. *Acc. Chem. Res.* **2000**, *33*, 27.
(3) Shon, Y.-S.; Choo, H. Organic Reactions of Monolayer-Protected Metal Nanoparticles. In *Dendrimers and Nanosciences*; Astruc, D., Ed.; *Comptes Rendus Chimie* Elsevier: Paris, 2003; Vol. 6 , pp 1009−1018.
(4) Shon, Y.-S. Metal Nanoparticles Protected with Monolayers: Synthetic Methods. In *Dekker Encyclopedia of Nanoscience and Nanotechnology*; Taylor & Francis: New York, 2004; published on-line 12/14/2004, E-ENN-120034034.
(5) Maye, M. M.; Lou, Y.; Zhong, C.-J. *Langmuir* **2000**, *16*, 7520−7523.
(6) Wuelfing, W. P.; Zamborini, F. P.; Templeton, A. C.; Wen, X.; Yoon, H.; Murray, R. W. *Chem. Mater.* **2001**, *13*, 87.
(7) Kim, Y.; Johnson, R. C.; Hupp, J. T. *Nano Lett.* **2001**, *1*, 165.
(8) Boal, A. K.; Rotello, V. M. *J. Am. Chem. Soc.* **2000**, *122*, 734.
(9) Fullam, S.; Rao, S. N.; Fitzmaurice, D. *J. Phys. Chem. B* **2000**, *104*, 6164.
(10) Templeton, A. C.; Hostetler, M. J.; Kraft, C. T.; Murray, R. W. *J. Am. Chem. Soc.* **1998**, *120*, 1906−1911.
(11) Chen, S.; Murray, R. W. *Langmuir* **1999**, *15*, 682−689.
(12) Chen, S. *Langmuir* **1999**, *15*, 7551−7557.
(13) Paulini, R.; Frankamp, B. L.; Rotello, V. M. *Langmuir* **2002**, *18*, 2368−237.
(14) Büttner, M.; Belser, T.; Oelhafen, P. *J. Phys. Chem. B* **2005**, *109*, 5464−5467.
(15) Radu, G.; Memmert, U.; Zhang, H.; Nicolay, G.; Reinert, F.; Hartmann, U. *J. Phys. Chem. B* **2002**, *106*, 10301−10305.
(16) Sheibley, D.; Tognarelli, D. J.; Szymanik, R.; Leopold, M. C. *J. Mater. Chem.* **2005**, *15*, 491−498.
(17) Hicks, J. F.; Shon, Y.-S.; Murray, R. W. *Langmuir* **2002**, *18*, 2288−2294.
(18) Hao, E.; Lian, T. *Chem. Mater.* **2000**, *12*, 3392−3396.
(19) Chan, E. W. L.; Lee, D.-C.; Ng, M.-K.; Wu, G.; Lee, K. Y. C.; Yu, L. *J. Am. Chem. Soc.* **2002**, *124*, 12238−12243.
(20) Krasteva, N.; Krustev, R.; Yasuda, A.; Vossmeyer, T. *Langmuir* **2003**, *19*, 7754−7760.
(21) Zamborini, F. P.; Leopold, M. C.; Hicks, J. F.; Kulesza, P. J.; Malik, M. A.; Murray, R. W. *J. Am. Chem. Soc.* **2002**, *124*, 8958−8964.
(22) Krasteva, N.; Besnard, I.; Guse, B.; Bauer, R. E.; Mullen, K.; Yasuda, A.; Vossmeyer, T. *Nano Lett.* **2002**, *2*, 551−555.
(23) Joseph, Y.; Besnard, I.; Rosenberger, M.; Guse, B.; Nothofer, H.-G.; Wessels, J. M.; Wild, U.; Knop-Gericke, A.; Su, D.; Schlögl, R.; Yasuda, A.; Vossmeyer, T. *J. Phys. Chem. B* **2003**, *107*, 7406−7413.

10.1021/cm0518980 CCC: $33.50
Published on Web 12/02/2005

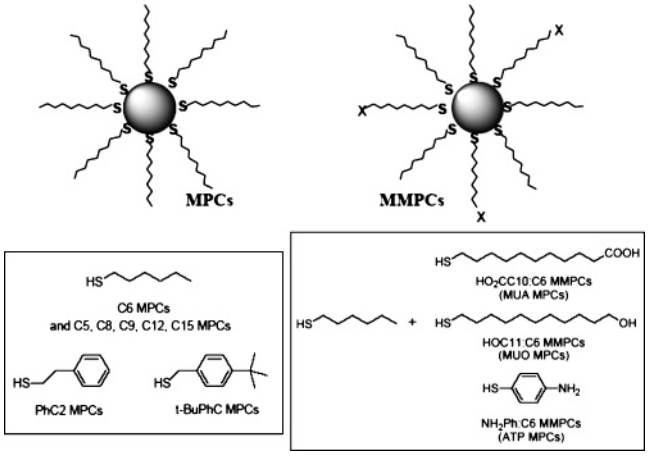

Figure 1. Various MPCs and MMPCs synthesized for the comparison of chemical and ultrasonic stabilities.

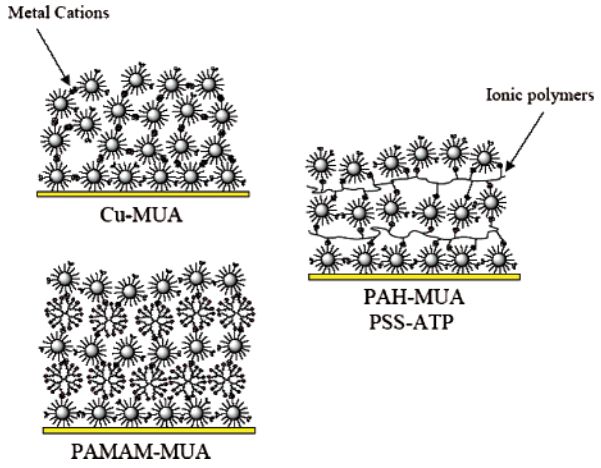

Figure 2. Nanoparticle multilayer assemblies prepared for the characterization of chemical, thermal, and ultrasonic stabilities.

metal nanoparticles offers the potential for application to semiconductor, photovoltaic, and molecular electronics fields. Many of the hybrid thin films have been created using a simple layer-by-layer self-assembly method. For example, COOH- or NH_2-functionalized MMPCs have been used for the preparation of nanoparticle multilayer films using linkers such as metal cations, ionic polymers, and dendrimers.[16−24] Applications using these hybrid films in chemiresistors or biological sensing have been reported by others.[20−24] Although understanding the stability of hybrid nanoparticle films is critical for technological applications of these materials, systematic research focusing on the stability of various nanoparticle multilayer films has rarely appeared.[25−27] We prepared several nanoparticle multilayer films, which were grown layer-by-layer by alternating exposures of reactive substrates to solutions containing MMPCs or linkers, to study their chemical, thermal, and ultrasonic stability (Figure 2). A further understanding of the chemical and physical properties of these nanostructures is important for exploiting the wide variety of applications such as chemical sensing, catalysis, and device applications.

Experimental Section

Materials. The following materials were purchased from the indicated suppliers, and were used as received. Hydrogen tetrachloroaurate ($HAuCl_4 \cdot 3H_2O$), copper perchlorate ($Cu(ClO_4)_2$), sodium borohydride ($NaBH_4$), and acetonitrile were obtained from Acros. 1-Pentadecanethiol, 1-dodecanethiol, 1-nonanethiol, 1-hexanethiol, 1-pentanethiol, 11-mercapto-1-undecanol, 11-mercapto-1-undecanoic acid, benzeneethanethiol, 4-*tert*-butylbenzylmercaptan, 4-aminothiophenol, polyallylamine hydrochloride (PAH; MW ca. 70 000), poly(sodium 4-styrenesulfonate) (PSS; MW ca. 70 000), polyamidoamine (PAMAM) [G-2], and tetraoctylammonium bromide were purchased from Aldrich. Ethyl alcohol, toluene, tetrahydrofuran (THF), acetone, glass microscope slides, and dichloromethane were obtained from Fisher. Water was purified by a Millipore Simplicity Nanopure Ultrapure water system.

Synthesis of MPCs. MPCs (average diameter core of ∼2.2 nm, average molecular formula of $Au_{314}L_{91}$) with monolayers composed of alkanethiolate (C5−C15) and benzeneethanethiolate (PhC2) ligands were synthesized using a modified Schiffrin reaction, the details of which are described in previous publications.[28,29] The standard procedure is as follows: 0.48 g (1.2 mmol) of $HAuCl_4 \cdot 3H_2O$ in 25 mL of Nanopure water was placed in the reaction flask. $AuCl_4^-$ was phase-transferred into toluene (50 mL) using 1.64 g (3.0 mmol) of tetraoctylammonium bromide (takes about 10 min), and the aqueous layer was discarded. Hexanethiol (0.28 g, 2.4 mmol) was added to the reaction mixture. The reaction mixture was stirred for ca. 10 min at room temperature, and 0.45 g (12.0 mmol) of $NaBH_4$ in 10 mL of Nanopure water was then added over a period of ca. 5 s. The solution quickly darkened during borohydride addition. After the solution was stirred for 3 h, the water phase was discarded, and the toluene was removed under vacuum, leaving a black solid. The black precipitate was suspended in 50 mL of acetonitrile, and was placed on a glass filtration frit. The product was exhaustively washed with acetonitrile and acetone.

The synthesis of 4-*tert*-butylbenzylmercaptan-protected MPCs (*t*-BuPhC2 MPCs) was done in a THF/H_2O single-phase solvent instead of a toluene/H_2O biphasic solvent.[30] The produced MPCs were exhaustively washed with acetonitrile. The *t*-BuPhC2 MPCs exhibit a high solubility in many organic solvents, including ethanol, hexane, and dichloromethane.

MPCs with average core dimensions of ∼3.2 and ∼4.4 nm with hexanethiolate monolayers were synthesized using a previously published method that can be found in the literature.[28c]

Synthesis of MMPCs. 11-Mercaptoundecanoic acid (MUA), 11-mercaptoundecanol (MUO), and 4-aminothiolphenol (ATP) ligands were incorporated into the monolayer shell using ligand-place-exchange reactions.[31] Briefly, the incoming functionalized alkanethiol- and hexanethiolate-protected gold clusters (C6 MPCs) were codissolved in methylene chloride; the approximate concentra-

(24) Yu, A.; Liang, Z.; Cho, J.; Caruso, F. *Nano Lett.* **2003**, *3*, 1203−1207.
(25) Prevo, B.; Fuller, J. C., III; Velev, O. D. *Chem. Mater.* **2005**, *17*, 28−35.
(26) Luo, J.; Maye, M. M.; Han, L.; Kariuki, N. N.; Jones, V. W.; Lin, Y.; Engelhard, M. H.; Zhong, C.-J. *Langmuir* **2004**, *20*, 4254−4260.
(27) Luo, J.; Jones, V. W.; Han, L.; Maye, M. M.; Kariuki, N. N.; Zhong, C.-J. *J. Phys. Chem. B* **2004**, *108*, 9669−9677.
(28) (a) Brust, M.; Walker, M.; Bethell, D.; Schiffrin, D. J.; Whyman, R. *Chem. Commun.* **1994**, 801. (b) Brust, M.; Fink, J.; Bethell, D.; Schiffrin, D. J.; Kiely, C. J. *Chem. Commun.* **1995**, 1655. (c) Hostetler, M. J.; Wingate, J. E.; Zhong, C.-J.; Harris, J. E.; Vachet, R. W.; Clark, M. R.; Londono, J. D.; Green, S. J.; Stokes, J. J.; Wignall, G. D.; Glish, G. L.; Porter, M. D.; Evans, N. D.; Murray, R. W. *Langmuir* **1998**, *14*, 17.
(29) Donkers, R. L.; Lee, D.; Murray, R. W. *Langmuir* **2004**, *20*, 1945−1952.
(30) Choo, H.; Cutler, E.; Shon, Y.-S. *Langmuir* **2003**, *19*, 8555−8559.
(31) Guo, R.; Song, Y.; Wang, G.; Murray, R. W. *J. Am. Chem. Soc.* **2005**, *127*, 2752−2757.

tion of the cluster was 2 mg/mL. The feed ratios[31] of the ligand-place-exchange reactions were 1:1 (MUA:SC6), 2:1 (MUO:SC6), and 1:1 (ATP:SC6). The solution mixture was stirred for 3 days, and the solvent was then removed under vacuum. The resulting precipitate was collected by filtration, and was washed with 100 mL of acetonitrile. The resulting mixed monolayers of the product MMPCs were determined via NMR spectroscopy. The NMR data showed the compositions of MMPCs to be approximately $Au_{314}(SC6)_{55}MUA_{36}$, $Au_{314}(SC6)_{32}MUO_{59}$, and $Au_{314}(SC6)_{73}ATP_{18}$. The NMR determination involves quantitatively desorbing the ligands from the MPC core as disulfides by addition of a crystal of iodine to the MPC solution.[30]

Functionalization of Glass Slides. The silanization procedure starts with glass microscope slides that have been cleaned in a "piranha" solution (3:1 H_2SO_4/H_2O_2), rinsed thoroughly with distilled water, and placed in 100 mL of an isopropyl alcohol solution containing 1 mL of the 3-mercaptopropylsiloxane and 1 mL of Nanopure water. After being heated for 30 min, the glass slides were rinsed with ethanol, blown dry with N_2, and allowed to dry in a 100 °C oven for at least 30 min. These previous processes (heating, washing, and drying) were repeated at least two more times. The prepared glass slides were stored in a dry cabinet for future use.

Layer-by-Layer (LbL) Assembly of Nanoparticle Multilayer Films. For the multilayers containing metal linkers, we prepared 0.1 M copper perchlorate ethanol solution. For multilayers containing polymer linkers, 10 mg of each polymer (PAH and PSS) was dissolved in 10 mL of Nanopure water, yielding ca. 14 μM solution concentrations. The polymer solution pH values were adjusted to 9.2 (PAH) and 1.4 (PSS) with 0.1 M NaOH and HCl solutions, respectively.[17] For multilayers containing dendrimer linkers, a 0.1 M polyamidoamine (PAMAM) [G-2] methanol solution was used. The ca. 30 μM MPC solutions used in the buildup of multilayers were made by dissolving 10 mg of each MPC (MUA and ATP MPCs) in 10 mL of pure ethanol. Multilayer films of nanoparticles were systematically and controllably grown layer-by-layer by alternating exposures of functionalized glass substrates to the solutions containing functionalized nanoparticles or linkers. Cu−MUA films were obtained by alternately exposing a glass surface to ethanolic solutions of $Cu(ClO_4)_2$ and to MUA MPCs. The second multilayer film was generated by alternately exposing the surface to an aqueous solution of PAH and to a solution containing MUA MPCs. This multilayer film is abbreviated PAH−MUA. The third multilayer film was generated by alternately exposing the surface to a methanolic solution of PAMAM [G-2] and to MUA MPCs. This multilayer film is abbreviated PAMAM−MUA. The fourth multilayer film was generated by alternately exposing the surface to an aqueous solution of PSS and to a solution of ATP MPCs. This multilayer film is abbreviated PSS−ATP. In Cu−MUA, PAH−MUA, and PAMAM−MUA films, the nanoparticles are neutral or anionic; in PSS−ATP films, they are cationic. The LbL procedure was repeated five times for all nanoparticle multilayer films, resulting in the formation of five bilayer assemblies.

Thermogravimetric Analysis (TGA). The TGA was conducted on a TA instruments TGA 2950 using an ultrahigh purity (UHP) nitrogen atmosphere (flow rate of 50 mL/min), with heating from room temperature to 600 °C at a heating rate of 20 °C/min.

Chemical Treatment of Nanoparticles and Nanoparticle Films. To 3 mL of a solution of MPCs in THF (final concentration of ~7.1 μM in clusters) was added 0.5 mL of NaCN in H_2O. The decomposition was carried out under normal conditions in ~8.7 mM NaCN. After brief agitation of the solution, the absorbance readings were minimized using a Shimadzu UV-2101 PC UV−vis spectrophotometer. Color change was present, as the brown−purple solution of MPCs decomposed into a colorless solution of AuCN complexes.[11,12]

The chemical stability of nanoparticle multilayer films was studied by monitoring the changes in the absorbance of nanoparticle films on glass by a UV−vis spectrophotometer before and after the immersion of nanoparticle films in the solutions containing chemical reagents such as 0.1 M HCl and 0.1 M KOH.

Thermal Treatment of Nanoparticle Films. The thermal stability of nanoparticle multilayer films was studied by monitoring the changes in the absorbance of nanoparticle films by a UV−vis spectrophotometer before and after the heating treatment of nanoparticle films in an oven under air. The controlled temperature was set to 100 ± 5 °C.

Ultrasonic Irradiation Treatment of Nanoparticles and Nanoparticle Films. The ultrasonic stabilities of nanoparticles and nanoparticle films were studied by monitoring the change in absorbance of nanoparticles dissolved in THF and nanoparticle films on glass in 30 mL of an acetonitrile solution, respectively, by a UV−vis spectrophotometer. The results obtained before and after the ultrasonic irradiation treatment of each sample were compared. The ultrasonic irradiation of all samples was conducted in a continuous mode with an Ultrasonic Generator UG 1200 made by Hanil Ultrasonic Co., Ltd. The ultrasonic equipment employed in this research had a frequency of 20 kHz and a power of 750 W. The configuration of the equipment was a horn-type system, and the size of the horn tip was 13 mm in diameter. The horn of the ultrasonic generator system was placed in a large reaction container, with the horn partially immersed in the solution (H_2O). The vial containing 10 mL of a THF solution with either MPCs or a glass slide with nanoparticle multilayer films was placed in the reaction container. The vial was not in direct contact with the horn (they were at least 6 cm apart). The temperature was maintained between 25 and 43 °C for all ultrasonic irradiation treatments. Both MPCs and nanoparticle films were stable at temperatures below 50 °C. The ultrasonic power per unit volume of MPC solution was 75 W/mL.

Results and Discussion

Thermogravimetric Analysis of MPCs and MMPCs. The TGA results of alkanethiolate (C5, C6, C8, C9, C12, and C15)-protected Au clusters revealed single and well-defined thermal decompositions (mass losses) of the alkanethiolate chains from the nanoparticle core (~2.2 nm). The mass losses were 13.9 (C5), 15.4 (C6), 18.4 (C8), 20.3 (C9), 24.9 (C12), and 28.8% (C15), which correspond to a quantitative loss of the organic monolayer as disulfides.[32] The TGA data also provide the temperature range at which the removal of the organic shell occurs. This evolution involves the formation of naked nanoparticles and, eventually, a bulk gold. The temperature dependence of the mass losses of the alkanethiolate-protected Au clusters was examined by comparing the peak maximum temperatures ($T_{max,DTG}$) of derivated thermogravimetic (DTG) peaks.[33] The $T_{max,DTG}$ values of these MPCs are shown in Table 1. These results clearly show that the monolayer with a longer alkyl chain required a higher temperature for the complete mass

(32) Terrill, R. H.; Postlethwaite, T. A.; Chen, C.; Poon, C.-D.; Terzis, A.; Chen, A.; Hutchison, J. E.; Clark, M. R.; Wignall, G.; Londono, J. D.; Superfine, R.; Falvo, M.; Johnson, C. S., Jr.; Samulski, E. T.; Murray, R. W. *J. Am. Chem. Soc.* **1995**, *117*, 12537−12548.
(33) Xie, W.; Xie, R.; Pan, W.-P.; Hunter, D.; Koene, B.; Tan, L.-S.; Vaia, R. *Chem. Mater.* **2002**, *14*, 4837−4845.

Table 1. Relative Mass Loss (TGA), Max Decomposition Temperature of Derivated TG, and Cyanide Decomposition Kinetics of Various MPCs and MMPCs

MPC[a]	% mass loss	$T_{max,DTG}$ (°C)	k (M^{-1} s^{-1}) [b]
C5 MPC	13.9	200.11	
C6 MPC	15.4	208.71	0.170 ± 0.005
C8 MPC	18.4	219.19	
C9 MPC	20.3	236.25	
C12 MPC	24.9	276.74	
C15 MPC	28.8	306.75	0.113 ± 0.007
PhC2 MPC			0.195 ± 0.018
t-BuPhC MPC	37.8	254.04	0.959 ± 0.037
HO_2CC10:C6 MMPC	17.8	120−450	0.307 ± 0.031
HOC11:C6 MMPC	19.2	150−400	0.752 ± 0.033
H_2NPh:C6 MMPC	13.2	173.95	0.647 ± 0.032

[a] The average core size of nanoparticles is ~2.2 nm ($Au_{314}L_{91}$). [b] Rate constants for the NaCN-induced decomposition of MPCs. Error bars are the standard deviation of the solution absorbance data from a first-order fit.

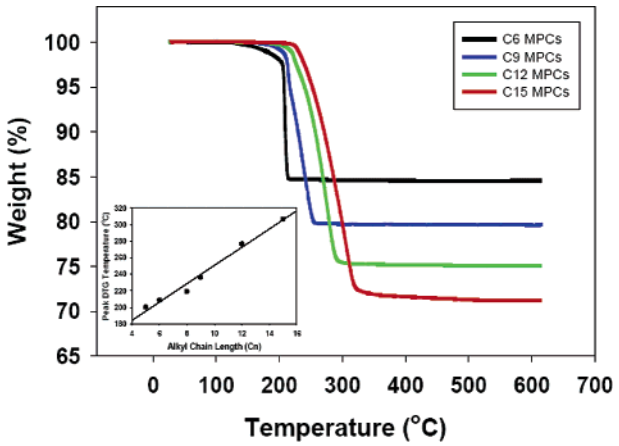

Figure 3. TGA data of alkanethiolate-protected Au clusters (C5−C15 MPCs). The inset shows the DTG decomposition temperatures of various MPCs (the *x*-axis is the alkyl chain length and the *y*-axis is the peak DTG temperature).

losses, which agrees with the previously published results (C8, C12, and C16 MPCs were compared).[32] In addition, our results suggest that the temperature for complete mass losses increases linearly with the increase in the alkyl chain length of protecting organic monolayers (inset of Figure 3). The result also shows that *t*-BuPhC MPCs (total of 11 Cs) exhibited a $T_{max,DTG}$ of 254.04 °C, which is close to the projected decomposition temperature of C11 MPCs. The TGA data for MMPCs, which were prepared by the ligand-place-exchange reaction of C6 MPCs, are shown in Table 1. The results show that the thermal decomposition of MUA MPCs (~120−450 °C) and MUO MPCs (~150−400 °C) showed broader decomposition regimes rather than individual decomposition steps. Compared to these data, the mass losses of ATP MPCs occurred almost in a single step, and the $T_{max,DTG}$ was observed at 173.95 °C. The results suggest that the presence of long-chain thiols such as MUA and MUO tends to broaden decomposition regimes, and a higher thermal energy is required for complete decomposition of the monolayers. This is probably due to the fact that the complete mass losses of monolayers are affected not only by the molecular mass of the each ligand but also by the interaction between the ligands present on a cluster surface.[13]

Stability of MPCs and MMPCs. The chemical stability of MPCs and MMPCs was studied by cyanide decomposition

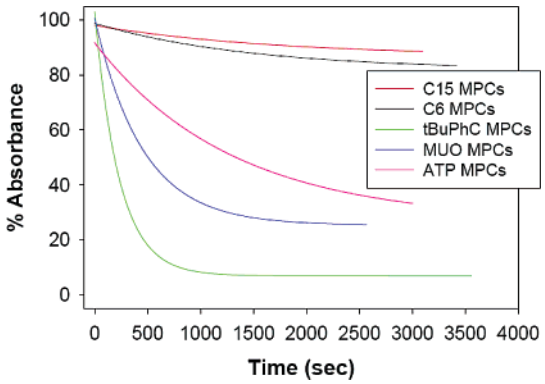

Figure 4. Normalized absorbance decay at 520 nm caused by NaCN-induced decomposition of MPCs and MMPCs.

reactions, which the rate of core decay indicated was a measure of core protection (Figure 4 and Table 1).[10−13] Cyanide causes the dissociation of the monolayer with concomitant etching of the gold underlayer, which yields disulfide products and colorless cyano−gold complexes.[11,12] The progress of the decomposition reaction could be monitored with UV−vis spectroscopy. It has been found that the reaction is first-order in the concentrations of both the clusters and the cyanide in solution. The absorbance decay data are fit to a general first-order equation, $y = y_0 + ae^{-kt}$, where y is the experimental absorbance and y_0 is a constant term accounting for a small amount of absorbance and/or light scattering by the reaction product. Figure 4 shows a first-order fit of the solution absorbance data of the surface plasmon (SP) band of gold at 525 nm. Table 1 gives the kinetic rate constants for decomposition reactions of various MPCs and MMPCs. The results show that the decomposition of C6 MPCs was more rapid than that of C15 MPCs, as previously reported.[10] Longer alkyl chains should provide a greater steric barrier and a thicker hydrophobic shell that resists ionic penetration. The rate constant of PhC2 MPCs was found to be greater in value than that of C6 MPCs. This result also agrees with the previous report about a relative stability of arenethiolate-protected gold clusters.[11] These results showed that the decomposition rate constants of arenethiolate-protected MPCs are, overall, greater in value than those of alkanethiolate-protected MPCs. It has been suggested that the interaction between the phenyl moiety and the cyanide ion caused the differential partition of cyanide ions into the monolayer shells. It was also suggested that the close packing of phenyl groups was more difficult than that of linear alkyl chains. This may cause a higher percentage of defect sites on gold nanoparticle surfaces and easier CN^- penetration, which results in faster decomposition of MPCs. We studied the CN decomposition of *t*-BuPhC MPCs, and found that these MPCs decomposed much faster than the other MPCs studied here. It has been reported that a bulky group (*tert*-butyl) caused a steric destabilization of monolayers on the particles rather than resulting in a steric hindrance to the gold core by forming a more-compact layer.[13] This caused a faster kinetic decomposition of nanoparticles by incoming CN ions.

The CN decomposition of MMPCs generated from C6 MPCs by ligand-place-exchange reactions suggests that the presence of functional groups such as OH or COOH caused

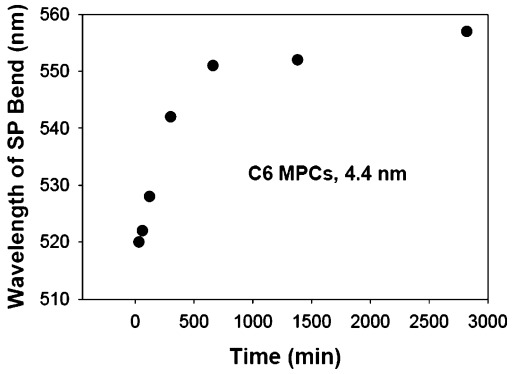

Figure 5. Change in the wavelength of the SP band of C6 MPCs upon ultrasonic irradiation.

a lowering of the chemical stability of MMPCs. Compared to C6 MPCs, MUO MPCs and MUA MPCs decomposed at least 2−3-fold faster. The presence of aminothiophenol (ATP) in C6 MPCs also dramatically lowered the chemical stability of MPCs. A comparison of the kinetic rates of decomposition between PhC2 MPCs and ATP MPCs shown in Table 1 also suggests that the presence of amine functional groups had a somewhat negative effect on the chemical stability of MPCs, which resulted in the faster decomposition of ATP MPCs than of PhC2 MPCs.

The ultrasonic stability of MPCs and MMPCs was studied by exposing nanoparticle solutions to ultrasonic irradiation, and then monitoring the changes in UV−vis spectra over time. The results showed that the ultrasonic stability of MPCs was largely affected by the chain length of surrounding organic monolayers. Nanoparticles protected with alkanethiols having longer alkyl chains (C9, C12, and C15 MPCs) were stable through 24 h of ultrasonic irradiation treatments. These MPCs did not undergo any significant change in their properties, which was evidenced by having the same wavelength and absorbance of the gold SP band at ∼520 nm. However, UV−vis spectra of C6 MPCs showed a visible change after ultrasonic irradiation treatments. As shown in Figure 5, the ultrasonic irradiation treatments of ∼4.4 nm C6 MPCs resulted in a red-shift of the SP band of gold from ∼520 to >550 nm in less than 10 h of exposure. Ultrasonic treatments of C6 MPCs with different core dimensions (∼2.2 and ∼3.2 nm) led to similar changes in the MPCs' UV−vis spectra. This result suggests that the aggregation of C6 MPCs under ultrasonic irradiation is independent of the size of the nanoparticles examined here. Surprisingly, ultrasonically treated MMPCs, including ATP MPCs and MUO MPCs, did not exhibit any changes in their UV−vis spectra, although these MMPCs were synthesized from C6 MPCs by ligand exchange. The results suggest that the presence of exchanged thiols with aromatic moieties or polar functional groups might improve the ultrasonic stability of MMPCs. Other MPCs with aromatic moieties (PhC2 MPCs and *t*-BuPhC MPCs) were also stable under ultrasonication. These results indicate that the chemical and ultrasonic stability of MPCs and MMPCs are relatively independent of each other. This is due to the intrinsic difference in the reaction mechanisms of these two different treatments. The CN decomposition involves an intercalation of CN ions into the monolayers and an etching of the nanoparticle core. Therefore, the packing of monolayers and the presence of defects on the cluster surfaces are relatively important for determining the chemical stability of MPCs. In the ultrasonic stability of MPCs, vibrational energy generated from ultrasonic irradiation is transferred to the materials as a kinetic energy. This causes the partial desorption of monolayers and the aggregation of nanoparticles. In this case, aggregation of nanoparticles is largely controlled by the lability of the ligands, which depends both on the strength of interaction between the ligand and surface and on the molecular weight of each ligand. As hexanethiolate ligands of C6 MPCs have the lowest molecular weight among the ligands of MPCs and MMPCs studied here, it is reasonable to see a lower stability in C6 MPCs compared to other MPCs and MMPCs.

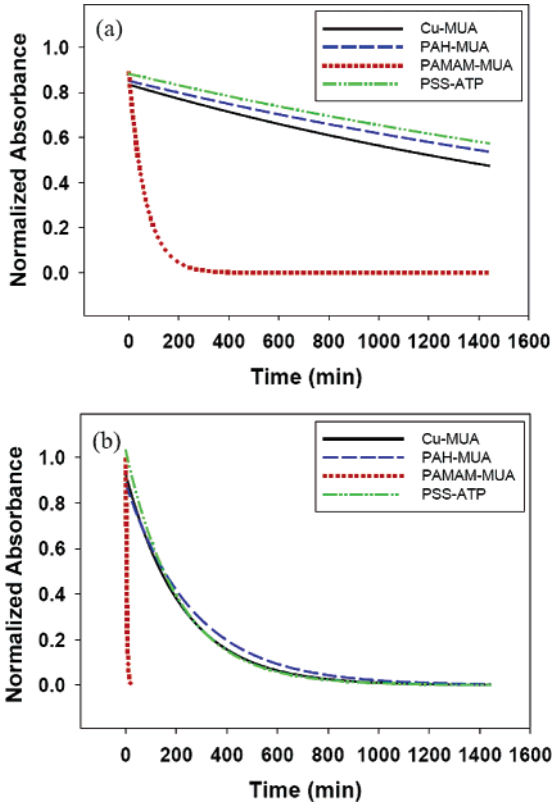

Figure 6. Chemical treatment of hybrid nanoparticle multilayer films with (a) 0.1 M HCl and (b) 0.1 M KOH solutions.

Stability of Nanoparticle Multilayer Films. The understanding of chemical and physical properties of assembled nanoparticle films is important for exploiting the unique applications of these materials. Herein, we report findings of spectroscopic investigations of the chemical, thermal, and ultrasonic treatments of nanoparticle multilayer assemblies with different linkers as a model system. In a UV−vis experiment, we monitored the change in absorbance intensity and the shift in the SP band, which is related to internanoparticle spatial, particle aggregation, and surrounding medium properties.[26] The LbL films were grown on the surface of reactive glass substrates. The wavelength of the SP band of gold showed a subtle increase and broadening toward the longer-wavelength region from ∼520 to ∼550 nm with increasing film thickness, as previously reported.[11] To understand the chemical stability of nanoparticle multilayer assemblies, we treated these assemblies with 0.1 M HCl and KOH solutions. An acid (HCl) and a base (KOH) disrupted

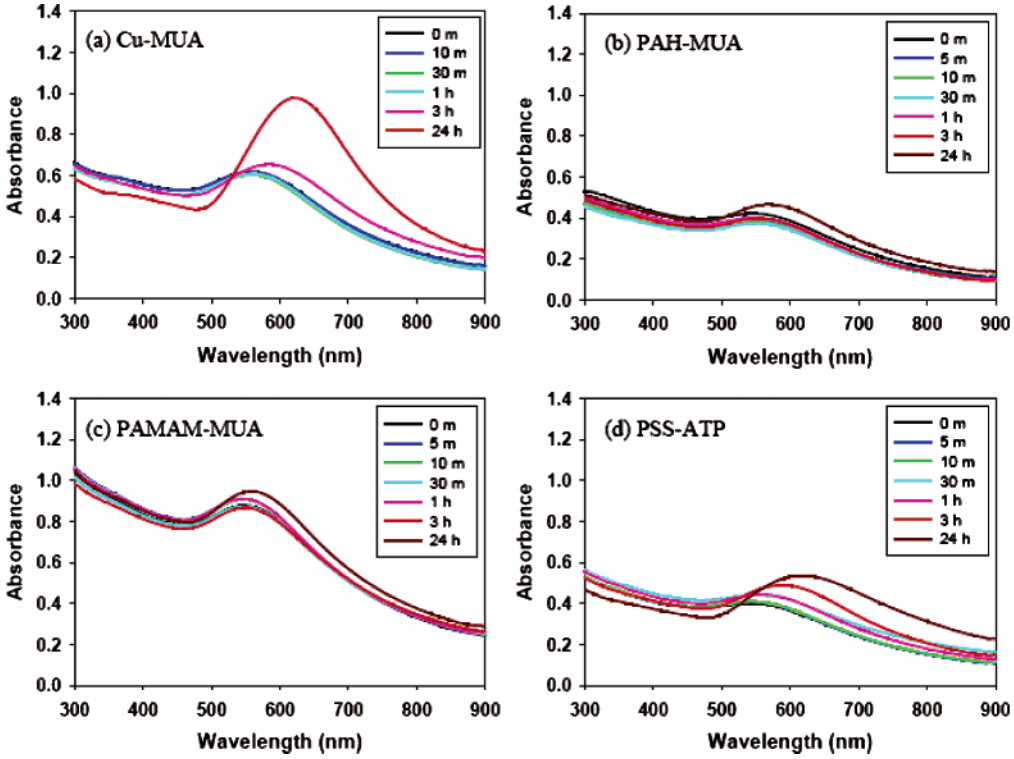

Figure 7. Thermal treatment of hybrid nanoparticle multilayer films at 100 °C.

the interaction between functionalized nanoparticles (MMPCs) and linkers (metals, polymers, or dendrimers), resulting in the loss of electrostatic, ionic, and/or hydrogen-bonding interaction between layers. These acid or base treatments caused a partial or complete desorption of nanoparticle multilayers. The intensity of the SP band of gold decreased with the loss of partial nanoparticle films from the glass surfaces. Figure 6 shows the UV−vis results of the absorbance change at 550 nm for the four hybrid nanostructures shown in Figure 2. The data were fitted using the equation $y = ae^{-kt}$.[34] The results suggest that PAH−MUA films (2.98×10^{-4} M^{-1} s^{-1}) were more stable than other nanoparticle multilayer assemblies in the acidic condition, on the basis of the kinetic rates of desorption. The PSS−ATP films (3.20×10^{-4} M^{-1} s^{-1}) also showed an overall stability quite comparable with that of PAH−MUA films. However, PAMAM−MUA films (1.49×10^{-2} M^{-1} s^{-1}) desorbed rather quickly. This result suggests that the polymer-linked nanoparticle films are more stable than dendrimer-linked nanoparticle assemblies. This is probably due to the entropy effect, which requires a simultaneous and multiple dissociation of linking groups for the desorption of nanoparticle films of PAH−MUA and PSS−ATP. PAMAM−MUA films were less stable because the number of linking groups dissociated during the desorption process is much smaller than that of polymer linkers. The chemistry of the desorption of Cu−MUA films is a little different than that of other multilayer assemblies. The interaction between nanoparticles and linkers in this case is based on a metal−organic coordination bond (or electrostatic interactions) rather than on acid−base interactions. A HCl solution could still disrupt this kind of bond effectively, resulting in a desorption of Cu−MUA films (3.91×10^{-4} M^{-1} s^{-1}) with a kinetic rate of desorption comparable to that of other polymer-linked nanoparticle multilayer assemblies. Under basic conditions (0.1 M KOH), the kinetic rates of the desorption of PAH−MUA films (3.76×10^{-3} M^{-1} s^{-1}), PSS−ATP films (4.80×10^{-3} M^{-1} s^{-1}), and Cu−MUA films (4.44×10^{-3} M^{-1} s^{-1}) were faster than those of nanoparticle multilayer assemblies under acidic conditions (0.1 M HCl). The PAMAM−MUA films (2.65×10^{-1} M^{-1} s^{-1}) again underwent the fastest desorption of films among the nanoparticle multilayer assemblies examined.

In a number of recent studies, thermal treatment of nanoparticle assemblies was attempted with focuses on preparing highly conductive films and surface-imbedded nanoparticle catalysts.[6,26,27] These include thermolysis of metal−carboxylate-linked gold nanoparticles,[6] hydrogen-bonding-induced nanoparticle assemblies,[26,27] and alkyldithiol-linked gold nanoparticle assemblies[34,35] at temperatures above 250 °C. In this study, we focused on heat treatments of nanoparticle multilayer films at a relatively low temperature (100 °C) to see the thermal stability of nanoparticle films in a more practical environment for technological applications. The structural evolution of the various nanoparticle assemblies treated at 100 °C under an ambient atmosphere was probed by UV−vis spectroscopy. It is known that heat treatments of nanoparticle films at high temperatures (>250 °C) result in the removal of organics and the formation of bare gold films or wires on solid substrates.[6,26,27] Our study showed that heat treatments of nanoparticle multilayer assemblies at 100 °C caused a morphological change in films rather than a desorption of nanoparticle films or a formation of thermolyzed gold films, which should result in a lowering of absorbance and a damped SP optical feature, respectively,

(34) Shon, Y.-S.; Lee, T. R. *J. Phys. Chem. B* **2000**, *104*, 8192−8200.

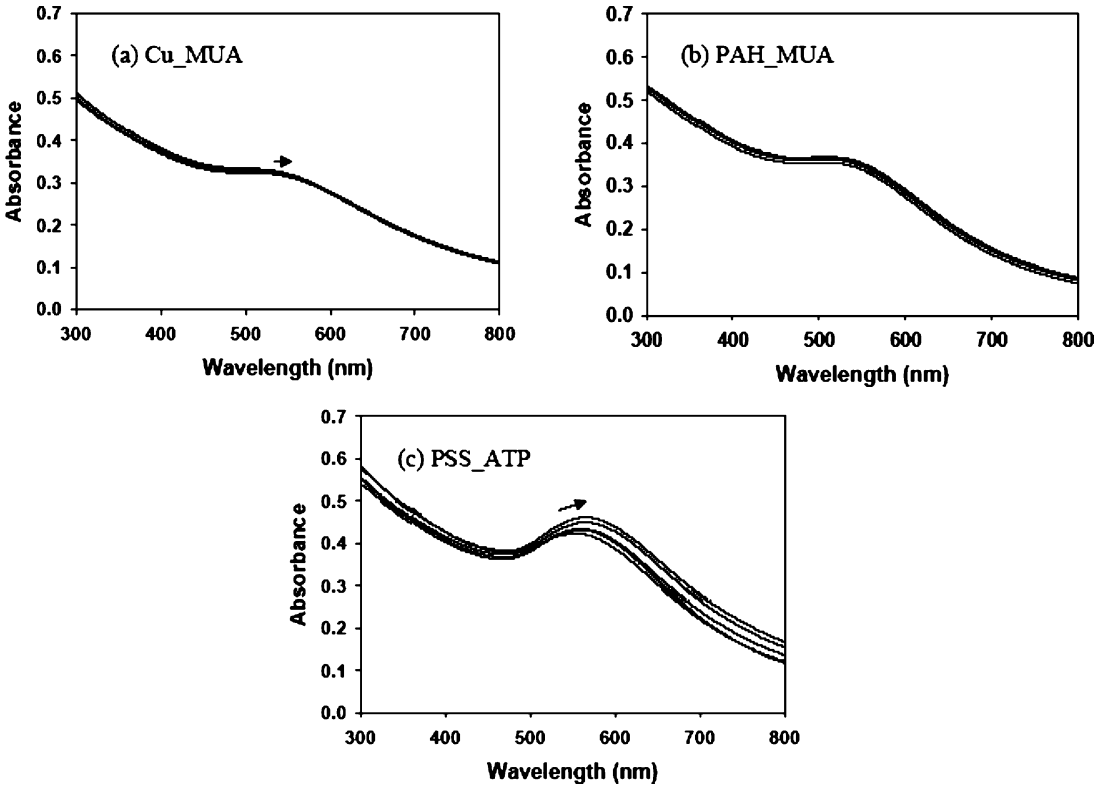

Figure 8. Ultrasonic irradiation treatment results for hybrid nanoparticle multilayer films. Irradiation time intervals (looking at curves from left to right or from bottom to top) are +10 min, +10 min, +10 min, +30 min, +1 h, +1 h, +1 h, +1 h.

in UV−vis spectra.[6] Instead, the SP band evolution revealed an initial increase in absorbance and a change in the band position with band broadening toward a longer wavelength (Figure 7). The band evolution is likely due to a combination of changes in particle size and interparticle distance.[26] Our observations indicated that the thermally induced structural evolution of nanoparticle multilayer assemblies was dependent upon the chemical nature of linkers. For Cu−MUA films, a large spectral evolution was observed, which was indicated by a dramatic increase in intensity of the SP band with a band broadening and shift toward a longer wavelength (>600 nm). PAH−MUA films exhibited a high stability against heat treatment at 100 °C. The multiple linkage that formed between polymer linkers and MPCs likely made the diffusion of nanoparticles in the polymeric matrix more difficult. The UV−vis spectra of PAMAM−MUA films showed a degree of SP band evolution that is quite comparable with that of PAH−MUA films after heat treatment at 100 °C, suggesting that the diffusion and aggregation of nanoparticles on the surface were not as easy as those of Cu−MUA films. PSS−ATP films showed SP band evolution that is more prominent than that of PAH−MUA films but less than that of PAMAM−MUA films. The SP band of PAH−MUA films shifted only <20 nm after 24 h of heat treatments. This shift was much smaller than the SP band shift observed from the UV−vis spectra of PSS−ATP films, which was ∼70 nm after heat treatments for 24 h. This difference is most likely caused by the difference in chemical structure between the two polymers PAH and PSS. PSS has a more rigid aromatic moiety, which could provide more open spaces in their packing structure. The open space in PSS−ATP can provide a much higher mobility of nanoparticles and a greater possibility of MPC−MPC contacts (aggregation). Previously, a higher mobility of electrolyte ions and a greater electronic-charge-transport behavior were observed for PSS−ATP films compared to that of PAH−MUA films.[17]

It was anticipated that prolonged exposure of nanoparticle films to ultrasonic irradiation could force deterioration of nanoparticle films. The ultrasonic stability of hybrid nanoparticle films was studied, and the results are shown in Figure 8. Prolonged ultrasonic irradiation of PAH−MUA films did not result in any visible change in UV−vis spectra, even after more than 5 h of exposure to ultrasonic irradiation. The UV−vis data for MUA−Cu films showed only a small (<5 nm) shift of the SP band of gold, without any change in the intensity of the SP band of gold. In comparison, the ultrasonic irradiation of PSS−ATP films resulted in a clearly visible red-shift of the SP band of gold, with an increase in the band intensity. This indicated that PSS−ATP films underwent morphological changes such as particle aggregation and/or particle nucleation on the surface during the ultrasonic irradiation treatment. As we observed from the results of the heat treatment of nanoparticle multilayer assemblies, these results show that the vibration of nanoparticle films causes a little faster aggregation of nanoparticles on the surface when the linkers are structurally less dense and have room for nanoparticle diffusion.

Conclusion

We have shown that the structure and functionality of a monolayer surrounding a nanoparticle core controlled both the chemical stability and ultrasonic stability of monolayer-protected nanoparticles. Cyanide decomposition of mono-

layer-protected nanoparticles suggested that the presence of polar functional groups or aromatic moieties lowered the chemical stability of nanoparticles. Ultrasonic irradiation of nanoparticles stabilized by hexanethiols resulted in the aggregation of nanoparticles. However, the presence or incorporation of long-chain alkanethiols and arenethiols enhanced the ultrasonic stability of monolayer-protected nanoparticles. An investigation of the chemical, thermal, and ultrasonic treatments of nanoparticle multilayer assemblies suggested that the structure and functionality of linker molecules governed the overall stability. Under both acidic and basic conditions, polymer and metal linkers provided a higher chemical stability than dendrimer linkers. After heat treatments at 100 °C, the UV−vis spectra of nanoparticle multilayer films with Cu linkers showed the largest spectral evolution compared to those of other films with polymer or dendrimer linkers, indicating the fast morphological evolution of nanoparticle films. Nanoparticle multilayer films with poly(sodium 4-styrenesulfonate) linkers aggregated a little faster than the films with polyallylamine hydrochloride or polyamidoamine (PAMAM) [G-2] linkers because of the higher mobility of the nanoparticles in these films. The ultrasonic irradiation of nanoparticle multilayer films also showed that the nanoparticle films with poly(sodium 4-styrenesulfonate) linkers underwent morphological changes such as particle aggregation and/or particle nucleation on the surface.

Acknowledgment. This research was supported by grants from Kentucky Science and Engineering Foundation, NASA/Kentucky Space Grant Consortium, and Western Kentucky University (MCC/ARTP). We thank Dr. Wei-Ping Pan (WKU) for providing access to TGA.

Supporting Information Available: TGA data, ultrasonication results, NaCN decomposition results, and UV−vis spectra (pdf). This material is available free of charge via the Internet at http://pubs.acs.org.

CM0518980